Title

Structure of the C-terminal guanine nucleotide exchange factor module of Trio in an autoinhibited conformation reveals its oncogenic potential

Journal

Science Signaling, 12(569)

ISSN

1945-0877

Authors

Bandekar, Sumit J

Arang, Nadia

Tully, Ena S

et al.

Publication Date

2019-02-19

DOI

10.1126/scisignal.aav2449

Peer reviewed

HHS Public Access

Author manuscript

Sci Signal. Author manuscript; available in PMC 2019 May 15.

Published in final edited form as:

Sci Signal. ; 12(569): . doi:10.1126/scisignal.aav2449.

Structure of the C-terminal guanine nucleotide exchange factor module of Trio in an autoinhibited conformation reveals its oncogenic potential

Sumit J. Bandekar[1,2], **Nadia Arang**[4,5], **Ena S. Tully**[2,3,#], **Brittany A. Tang**[2,3,#], **Brenna L. Barton**[2,3,#], **Sheng Li**[7], **J. Silvio Gutkind**[4,6], and **John J.G. Tesmer**[8,*]

[1]Department of Medicinal Chemistry, University of Michigan, Ann Arbor, MI 48109

[2]Life Sciences Institute, University of Michigan, Ann Arbor, MI 48109

[3]Department of Pharmacology, University of Michigan, Ann Arbor, MI 48109

[4]Moores Cancer Center, University of California San Diego, La Jolla, California, 92093

[5]Biomedical Sciences Graduate Program, University of California, San Diego, La Jolla, CA 92093, USA

[6]Department of Pharmacology, University of California San Diego, La Jolla, California, 92093

[7]Department of Medicine, University of California San Diego, La Jolla, California, 92093

[8]Departments of Biological Sciences and of Medicinal Chemistry and Molecular Pharmacology, Purdue University, West Lafayette, Indiana, 47907

Abstract

The C-terminal guanine nucleotide exchange factor (GEF) module of Trio (TrioC) transfers signals from the $G\alpha_{q/11}$ subfamily of heterotrimeric G proteins to the small guanosine triphosphatase (GTPase) RhoA, enabling $G\alpha_{q/11}$-coupled G protein–coupled receptors (GPCRs) to control downstream events, such as cell motility and gene transcription. This conserved signal transduction axis is crucial for tumor growth in uveal melanoma. Previous studies indicate that the GEF activity of the TrioC module is autoinhibited, with release of autoinhibition upon $G\alpha_{q/11}$ binding. Here, we determined the crystal structure of TrioC in its basal state and found that the pleckstrin homology (PH) domain interacted with the Dbl homology (DH) domain in a manner that occludes the Rho GTPase binding site, thereby suggesting the molecular basis of TrioC autoinhibition. Biochemical and biophysical assays revealed that disruption of the autoinhibited conformation destabilized and activated the TrioC module in vitro. Finally, mutations in the DH-

*Corresponding author. jtesmer@purdue.edu.

Author contributions: S.J.B, N.A., J.S.G., and J.J.G.T. conceptualized the study. S.J.B, N.A., J.S.G., and J.J.G.T. designed the methodology. S.J.B. and N.A., with the assistance of B.A.T, E.S.T, and B.L.B., performed the experimental investigations. S.L. collected and processed the HDX-MS data. S.J.B. wrote the original draft and S.J.B, N.A., J.S.G., and J.J.G.T. revised the manuscript text. S.J.B., N.A., J.S.G., and J.J.G.T. contributed funding to the study.

#These authors contributed equally to this manuscript.

Competing interests: The authors declare that they have no competing interests.

Data and materials availability: The crystal structure of TrioC along with diffraction amplitudes has been deposited into the Protein Data Bank under accession code 6D8Z. Plasmids and other reagents are available upon reasonable request to J.J.G.T. All other data needed to evaluate the conclusions in the paper are present in the paper or the Supplementary Materials.

PH interface found in cancer patients activated TrioC and, in the context of full-length Trio, led to increased abundance of guanosine triphosphate–bound RhoA (RhoA·GTP) in human cells. These mutations increase mitogenic signaling through the RhoA axis and, therefore, may represent cancer drivers operating in a $G\alpha_{q/11}$-independent manner.

INTRODUCTION

Rho guanine exchange factors (RhoGEFs) are signaling modules that activate Rho-family small molecular weight GTPases (1, 2). These enzymes stabilize a nucleotide-free state of their cognate GTPases, thereby accelerating the process of nucleotide exchange. The C-terminal RhoGEF module of Trio (TrioC) regulates developmental and growth processes by influencing the actin cytoskeleton and gene transcription through activation of RhoA (3). TrioC and the related RhoGEF modules p63RhoGEF and KalirinC are downstream effectors of $G\alpha_{q/11}$ and thereby give rise to a chain of phospholipase C-β-independent events upon activation of $G\alpha_{q/11}$-coupled GPCRs (4-6). In >80% of cases, a constitutively active mutation in $G\alpha_{q/11}$ drives the progression of uveal melanoma (UM) in a Trio dependent fashion (7-9).

The prototypic RhoGEF module is composed of a Dbl homology (DH) and pleckstrin homology (PH) domain tandem linked by a flexible helix of variable length.(2,10) The DH domain is responsible for binding the nucleotide-free state of substrate GTPases, whereas the PH domain plays various roles ranging from enhancement of GEF activity, such as in Dbl's big sister (Dbs) and the N-terminal DH/PH module of Trio (TrioN), to suppression of GEF activity as in the TrioC subfamily. Regulation mediated by the PH domain is known to occur by one of several mechanisms, including protein-protein or lipid-protein interactions (11 16).

Structural and functional studies of p63RhoGEF, a close homolog of TrioC, show that $G\alpha_{q/11}$·GTP binds to both the DH and PH domains and thereby constrains the DH/PH module in a manner that optimizes the RhoA binding site. However, the structural basis for how the PH domain mediates autoinhibition in the TrioC subfamily remains unclear (6,17). Such information would enable a better understanding of how Trio contributes to cancer progression and pave the way for future therapeutics that could stabilize the less active, basal form of TrioC. There are currently no effective approved therapies for the treatment of UM (18).

In this study, we used X-ray crystallography to show that the TrioC PH domain inhibits GEF activity by forming an interface with the DH domain that blocks the binding site for switch II of RhoA. Using biochemical assays, we have demonstrated the importance of residues unique to TrioC, as well as subfamily members p63RhoGEF and KalirinC, in the N-terminal α-helix of the PH domain (αN) that contribute to the interface. Hydrogen-deuterium exchange mass spectrometry (HDX-MS) also supports a model wherein the RhoA binding site on the DH domain is occluded by the PH domain through contacts made by the observed DH-PH interface. Furthermore, we demonstrated that mutations found in the TrioC αN region in cancer patients not only activate the TrioC fragment in GEF assays, but also full-length Trio in human cells, allowing for sustained signaling through RhoA (19-21).

RESULTS

Crystal structure of the TrioC DH/PH module reveals its autoinhibited conformation

We determined the 2.65 Å crystal structure of the human TrioC module (Table 1). As in previously determined Dbl family DH/PH structures, the TrioC module begins with an α-helical DH domain, consisting of 6 helical spans (α1-α6; Fig. 1A). The α6 helix is continuous with the short first helix of the PH domain, αN, and their junction serves as a flexible hinge between the DH and PH domains. The remainder of the PH domain is composed of a seven-stranded (designated β1-β7) antiparallel β-sandwich capped on one end by a C-terminal helix (αC). Three copies of the TrioC module are found in each asymmetric unit (fig. S1A). They are similar in overall conformation with a mean root mean square deviation (RMSD) of 0.8 Å for Cα atoms (fig. S1B), with minor differences arising from unique crystal contacts.

The only other reported structure of a TrioC subfamily RhoGEF module is that of p63RhoGEF (65% sequence identity) in complex with $G\alpha_q$ bound to guanosine diphosphate and aluminum tetrafluoride ($G\alpha_q{\cdot}GDP{\cdot}AlF_4^-$) and nucleotide-free RhoA [Protein Data Bank (PDB) entry 2RGN], representing a TrioC subfamily member in its activated, signal competent state. In Dbs, a closely related RhoGEF with a PH domain that positively contributes to nucleotide exchange, the DH and PH domains adopt a conformation more similar to activated p63RhoGEF than to autoinhibited TrioC (Fig. 1, B and C). The region encompassing the α6/αN junction (Trio residues 2139-2150) in the TrioC structure adopts a less bent α-helical conformation, with the αN helix forming the bulk of the interactions with α3 in the DH domain (Fig. 1A, inset). The analogous αN elements in activated p63RhoGEF (Fig. 1B, inset) and Dbs (Fig. 1C, inset) are instead displaced from the DH domain, leaving space for switch II of RhoA to bind.

In TrioC, Gly^{2149} (Ile^{816} in Dbs; Fig. 1C, inset) packs against the side chain of Pro^{2066} in α3 of the DH domain, enabling closer proximity of the TrioC DH and PH domains (Fig. 1A, inset). Meanwhile, TrioC-Arg^{2150} forms an interdomain salt bridge with Glu^{2069} in α3, which is substituted by Ala^{817} in Dbs. The side chain of Met^{2146} also bridges the DH and PH domains by forming a hydrogen bond with the side chain of Arg^{2150} and hydrophobic contacts with the DH domain. These interactions are broken upon the binding of $G\alpha_q{\cdot}GDP{\cdot}AlF_4^-$, as seen in the active p63RhoGEF structure (Fig. 1B, inset). Glu^{2069}, Gly^{2149}, and Arg^{2150} are invariant in the TrioC subfamily, but not conserved in Dbs or the closely related N-terminal DH/PH modules of Trio and Kalirin (fig. S2). Met^{2146}, however, is conserved as a hydrophobic residue in most RhoGEFs that forms direct contacts with Switch II of bound GTPases.(11,22) Although not as highly conserved among TrioC subfamily members, residues 2204-2212 in the β3-β4 of the PH domain loop bury the Arg^{2150}-Glu^{2069} salt bridge and form additional interactions with α3 in the DH domain, including a hydrogen bond between the hydroxyl of Ser^{2208} and side chain of Glu^{2069}. In the active p63RhoGEF structure, β3-β4 is disordered (Fig. 1B). In Dbs, the equivalent loop is disordered without bound GTPase (Fig. 1C).

Aligning the core of the DH domain of TrioC (Trio residues 1967-2136, Chain A) with that of activated p63RhoGEF revealed a 60˚ relative rotation of their PH domains around the axis

of the α6-αN hinge (Fig. 2A).(11,22) This allows for the formation of an interface between the DH and PH domains of TrioC which overlaps with the RhoA binding surface of the DH domain, providing a likely mechanism for autoinhibition (Fig. 2A, inset). In particular, the α6-αN hinge region of TrioC also has a 30˚ bend relative to the active conformation of p63RhoGEF (Fig. 2B) so that a more standard linear helix is formed. This allows Glu^{2069} and Met^{2146}, which interact directly with RhoA in the activated p63RhoGEF structure, to instead directly engage Arg^{2150}. Whether in GTPase-bound or -free states, the α6-αN hinge in Dbs adopts a conformation most similar to that of activated p63RhoGEF (Fig. 2B). Thus, whereas the Dbs DH/PH module is prearranged for competent nucleotide exchange, the TrioC module adopts an autoinhibited conformation until $G\alpha_q$·GTP binds and changes the helical track of α6-αN so that the DH domain can bind RhoA.

Site-directed mutations in the DH-PH interface destabilize and activate TrioC

We hypothesized that variants which disrupted important contacts in the DH-PH interface would be more sensitive to thermal denaturation [meaning a lower melting temperature (T_m) relative to wild type (WT)], as measured by differential scanning fluorimetry (DSF), and display increased GEF activity. Thus, we introduced site-directed mutations into the α6-αN hinge, the β3-β4 loop, and α3. E2069A, M2146A, and S2208A variant proteins exhibited lower melting points by 3 to 7 ˚C, whereas R2150A and F2207A (β3-β4 loop) variants were 1 ˚C more thermostable than was WT TrioC (Table 2). These alanine variants also had a similar exchange rate to that of WT TrioC (Table 2). DSF and FRET assay results of β3-β4 loop-deletions Δ2204-2208 and Δ2203-2209 were similar to those of wild-type. A larger loop deletion, Δ2201-2211, yielded insoluble protein and could not be assayed. The G2149I variant, replacing the position with the cognate residue in Dbs, reduced the T_m over 6 ˚C and displayed 2-fold higher exchange relative to WT. The E2069R/R2150E double mutant, designed to test the importance of the salt bridge, destabilized protein 8 °C and activated 3-fold. Thus, the electrostatic complementarity of these positions is not as important as their contributions to the local structure. The single R2150E mutant was not significantly different from WT in terms of its nucleotide exchange activity or thermostability, whereas E2069R yielded insoluble protein and could not be assayed. Thus, the E2069R substitution is most likely responsible for the activation exhibited by the E2069R/R2150E double mutant, but it is only stable in the context of a salt bridge swap. We conclude from these results that mutations that introduced bulk or collisions in the closed interface (such as G2149I and E2069R/R2150E) had a greater ability to destabilize and activate the DH/PH module compared to mutations that simply remove contacts (such as R2150A).

Mutations found in cancer patients destabilize and activate the TrioC module

Analysis of the cBioPortal database (23) revealed that truncations 2152Δ (stop codon after residue 2152) and 2153Δ occur in human cancer patients. 2153Δ removes the bulk of the PH domain yet leaves αN intact. This variant activated the DH/PH module 3-fold relative to wild type TrioC (Table 2). 2152Δ activated the module 11-fold over WT. To assess the consequences of further truncation, we assayed 2147Δ, which removes all of αN and found that it was 14-fold activated. A final truncation, 2143Δ, which in addition removes a portion of α6, had ~5-fold lower GEF activity than WT, likely due to loss of RhoA binding residues. The cBioPortal database also contains the G2149W, R2150Q, and R2150W variants, which

we hypothesized would be activating due to steric or electrostatic disruption of the autoinhibited DH-PH interface. Indeed, we found that all had reduced T_m values and were >4-fold more active than WT (Table 2), consistent with a model wherein the PH domain must be dislodged from the DH domain in order to facilitate RhoA binding. We also found that G2149W and R2150Q could be activated by $G\alpha_q$ in an AlF_4^--dependent manner in the same assay format, although these two variants were activated to a lesser extent (~2 fold) than TrioC WT (~3-fold). Our most active TrioC variant, R2150W, was not activated by $G\alpha_q{\cdot}GDP{\cdot}AlF_4^-$ (Table 2), suggesting that there is an upper limit to activation of the intact DH/PH module. Truncation mutants of TrioC were not likewise tested because they lack the $G\alpha_q$ binding site.

HDX-MS shows higher dynamic behavior in the DH-PH interface in constitutively activated TrioC

We subjected R2150W and WT TrioC to HDX-MS experiments (fig. S3, A and B) to study activated and basal forms of the enzyme in solution. In the HDX-MS difference map R2150W-WT (Fig. 3 and fig. S3C), the regions in close proximity to the R2150W mutation exchanged backbone hydrogens more than in WT, and residues in α3 also display a marked increase in exchange, supporting the notion that these two regions directly interact in the autoinhibited, basal state. The β3-β4 loop exhibited no difference in exchange dynamics between the two states.

DH-PH interfacial mutants activate RhoA in mammalian cells

Full-length Trio is the primary splice variant transcribed, and thus likely the predominant variant expressed, in UM cell lines.(7) Thus we compared the activity of the cancer-associated variants, G2149W, R2150Q, and R2150W, to WT in the context of human Trio (residues 61-3097) under serum starved conditions to detect inherent Trio activity. Proteins were expressed as C-terminal enhanced green fluorescent protein (eGFP) fusions using transient transfection in human embryonic kidney 293 (HEK293) cells. Because 2152Δ was the most active truncation in vitro, it was also profiled. A pulldown assay using the Rho-binding domain of the RhoA effector Rhotekin (Cytoskeleton, Inc.) (7) was employed to determine the relative ratio of active RhoA (RhoA·GTP) to total RhoA content in response to expression of WT and mutant Trio. Expression of R2150W, R2150Q, G2149W, and 2152Δ Trio mutants all led to a >2-fold increase in the abundance of RhoA·GTP as compared to expression of WT Trio (Fig. 4A). All Trio variants were expressed to a similar extent (Fig. 4B and fig. S4).

DISCUSSION

The definition of the molecular events underpinning carcinogenic signaling in UM has showcased the role of Trio in transmitting signals from constitutively active $G\alpha_{q/11}$ subunits to the nucleus (7, 24). $G\alpha_{q/11}{\cdot}GTP$ activates Trio by relieving an autoinhibitory constraint on TrioC, which leads directly to nucleotide exchange of RhoA into its GTP-bound form. In this work, we have defined the structural basis of this autoinhibitory constraint using X-ray crystallography accompanied by HDX-MS and validated our model with biochemical and cell-based assays. The crystal structure of the TrioC module revealed the structure of a

DH/PH tandem in a conformation incapable of binding GTPase. All three copies of the protein in the asymmetric unit adopt a highly similar conformation, indicating that the observed configuration of the DH and PH domains is not an artifact of crystal packing. In other published crystal structures of Dbl family members, the DH and PH domains can exhibit distinct relative orientations (12,13,22), consistent with the α6-αN connecting region serving as a hinge. The crux of our structure is a novel interface formed between the α6-αN hinge region and the DH domain, with the most important contacts being made by residues in αN. It showed that Gly^{2149} and Arg^{2150} both make extensive contacts with the DH domain, with Gly^{2149} enabling closer proximity of αN to the DH domain than in other DH/PH modules, and Arg^{2150} sequestering DH domain residues Glu^{2069} and Met^{2146}, which both make contact with RhoA in the bound state. We determined that these residues are conserved among TrioC homologs in humans, but not in other RhoGEF modules including the N-terminal modules in Trio and Kalirin. The presence of Gly^{2149} and Arg^{2150} is likely a prerequisite for αN to follow a standard helical track at the end of α6 in order to block the switch II binding site of RhoA on the DH domain. Accordingly, mutations of Gly^{2149} and Arg^{2150} were generally activating. Mutation of the analogous residues in p63RhoGEF (Gly^{340} and Arg^{341}) were also activating (17), and we predict this trend would hold true for the KalirinC module. In contrast, the closely related PH domains of Dbs/TrioN instead enhance GEF activity by positioning residues in the α6-αN hinge region to form beneficial interactions with the GTPase substrate (11, 14). To the best of our knowledge, Sos1 is the only other example of a Dbl family structure in which the PH domain directly binds to the DH domain. In Sos1, the DH-PH interface involves the GTPase binding site of the DH domain and the αC helix of the PH domain. Given the poor conservation of the residues involved across the Dbl family, this interaction surface is likely unique to Sos1 (15, 25).

The TrioC 2153Δ, 2152Δ, and 2147Δ truncations were all activated relative to WT TrioC (Table 2). Thus, the basal activity of the DH domain is highly sensitive to whether the PH domain is present. The bulk of the PH domain, and in particular its extended C-terminal helical region, is also required for binding and activation by $G\alpha_q$-GTP (17).

Activation by truncation is a likely explanation for the transforming activity of Tgat, a splice variant of Trio encoding Trio residues 1921-2160 followed by a unique 15 residue extension (26). Although the WT α6-αN region in Tgat is entirely present, the lack of the core PH domain fold in this variant could mean that the αN helix is disordered and thus cannot confer full autoinhibition as we see in the 2153Δ and 2152Δ variants. Alternatively, the 15 residue extension could drive an activated conformation of the α6-αN hinge region by making unique contacts within the protein, with other signaling partners, or with the cell membrane (27-29).

Alanine scanning mutations throughout the DH-PH interface did not affect TrioC activity. In contrast, substitutions that introduced bulk into the interface such as G2149I/W, E2069R/R2150E, and R2150W were able to activate TrioC >2-fold. These data suggest that in the absence of the interactions formed by one side chain, as in the R2150A variant, the remaining residues in the DH-PH interface can still contact each other and stabilize the autoinhibited conformation. In contrast, variants which insert steric bulk into the interface will disrupt the majority of DH-PH interfacial contacts from forming.

Although the β3-β4 loop is resolved as part of the closed DH-PH interface in our crystal structure, this poorly conserved loop likely plays little to no role in the autoinhibition of TrioC family members. Its removal did not affect TrioC activity or thermostability, and our HDX-MS profiling of the active mutant R2150W showed no difference in exchange rates in the β3-β4 loop, which we would expect to see if this loop formed a part of the DH-PH interface. Instead, the crystal contacts that β3-β4 makes with neighboring TrioC monomers are likely responsible for its ordered conformation in the crystal structure. Truncation of the analogous loop in p63RhoGEF (Δ397-402) has no effect on activity (17). The β3-β4 loops in TrioN and Dbs make contacts with the bound GTPase, but mutation of the loop has no effect in vitro (11, 14).

Our data support a model wherein TrioC exists in an equilibrium of autoinhibited and active conformations (Fig. 5). The existence of an equilibrium is supported by the measurable basal GEF activity of TrioC and full-length Trio. The basal autoinhibited state is represented by the crystal structure we have reported here (Fig 5, top left quadrant). TrioC can sample a conformation which is active in the absence of $G\alpha_q$·GTP, and the cancer point variants we profiled are able to shift the equilibrium towards this state (Fig. 5, bottom left quadrant). This is accomplished through displacement of αN from its contacts with α3 (confirmed by HDX-MS). $G\alpha_q$·GTP binds primarily to an extension of αC in the PH domain (Fig. 5, top right quadrant) yet does not activate TrioC until it binds to both DH and PH domains and displaces αN from α3 (Fig. 5, bottom right quadrant, represented by PDB entry 2RGN). Our results suggest that because the cancer-associated point variants favor a conformation similar to that produced by $G\alpha_q$·GTP binding, they synergistically enhanced $G\alpha_q$·GTP binding and a maximum activation rate. The exception is R2150W, whose activity was not further enhanced by saturating $G\alpha_q$·GDP·AlF_4^-. This variant may be present in a fully activated conformation without need for $G\alpha_q$·GDP·AlF_4^-.

We posit that activation of TrioC by $G\alpha_q$·GTP, by point mutation, and by truncation all depend on the same biophysical mechanism: displacement of αN from the contacts made with α3 seen in our crystal structure. As is seen in our cell-based RhoA activation assay, this paradigm held true in an overexpression model of full-length Trio in human cells. Thus, in human cancer, Trio has the potential to bypass regulation by $G\alpha_{q/11}$ by truncation or point variation, which would lead to the activation of RhoA and downstream proliferative signaling through the AP-1 and YAP-TEAD axes (19, 24). A small molecule stabilizer of the autoinhibited TrioC conformation reported here could prove fruitful in halting proliferative signaling through Trio. In combination with therapies targeting the other arms of $G\alpha_q$ signaling, a TrioC inhibitor could be an effective part of a combination therapy for UM.

MATERIALS AND METHODS

Cloning and site-directed mutagenesis

All residue numbering in this manuscript is with respect to human Trio isoform 1, which is 3097 amino acids in length (UniprotKB O75962). Human TrioC complimentary deoxyribonucleic acid (cDNA) (Trio residues 1960-2290) was inserted into a modified pMAL expression vector (pMalC2H10T) (13) using restriction cloning. TrioCΔC (Trio 1960-2275) was also inserted into pMalC2H10T. TrioCΔC was designed based on the

prediction that the conserved C-terminal extension of the PH domain (residues 2275-2290) is likely disordered in the absence of $G\alpha_q$.(5) The RhoA construct was described previously (13). $G\alpha_q\Delta N$ was used in the activation assays and corresponds to residues 35-359 of murine $G\alpha_q$ (30). Site-directed mutants and deletions were generated on the TrioC template using an inverse polymerase chain reaction (PCR) or the Quikchange protocol from Agilent. TrioC cDNA was set in an inverse PCR reaction with Q5 polymerase (New England Biolabs (NEB)), and the PCR reaction was digested with Dpn1 (NEB), phosphorylated with T4 polynucleotide kinase (NEB), and ligated with T4 DNA ligase (NEB). The ligated plasmid was then transformed into XL1-Blue cells (Agilent), and the mutation was confirmed using Sanger sequencing of plasmid DNA purified using a Mini-prep kit (Qiagen). To generate variants in TrioFL-pEGFP (containing Trio residues 61-3097), a 1000 base pair fragment containing the mutations was PCR amplified from TrioC mutants in pMalC2H10T. Gibson assembly was used to join fragments to a fragment from TrioFL containing an additional restriction site. Final assembled fragments and TrioFL were then digested with SpeI and FseI and ligated to generate the full-length gene variants (reagents from NEB).

Protein expression and purification

Plasmids encoding TrioC variants and RhoA were transformed into Rosetta (DE3) pLysS *E. coli* cells (Novagen) and grown in Terrific Broth (EMD Millipore Sigma) with 100 μg/mL carbenicillin at 37 ˚C with 200 rpm shaking. Once a 600 nm optical density (OD_{600}) of 0.6-0.8 was reached, expression of N-terminally tagged maltose binding protein (MBP) fusion proteins was induced using 1 mM isopropyl β-D-1-thiogalactopyranoside and cells were further allowed to grow at 20 ˚C with 200 rpm shaking for 20 h. *E. coli* were then harvested at 5000 × g for 15 min and cell pellets were flash-frozen or prepared. Cell pellets were resuspended using a dounce homogenizer in an ice-cold “lysis buffer” containing 20 mM (4-(2-hydroxyethyl)-1-piperazineethanesulfonic acid) HEPES pH 8.0, 200mM NaCl, 2 mM dithiothreitol (DTT), 2 mM $MgCl_2$, 5% glycerol, 0.001 mM leupeptin, 1 mM lima bean trypsin inhibitor, and 0.1 mM phenylmethylsulfonyl fluoride. Resuspended cell solution was then lysed using an EmulsiFlex C3 homogenizer (Avestin), and deoxyribonuclease I (DNase I) or benzonase was added to remove excess nucleic acid. Lysate was then centrifuged at 32000 × g in an Avanti J-20 centrifuge (Beckman-Coulter) to remove insoluble material. The soluble fraction was then filtered through a glass fiber filter and loaded onto nickel-nitrilotriacetic acid (Ni-NTA) agarose resin (Qiagen) equilibrated with lysis buffer. Next, 10 column volumes (CV) of lysis buffer were used to wash the column, followed by a 10 CV wash of lysis buffer containing 20 mM imidazole and 300 mM NaCl. A final wash step consisted of 10 CV of lysis buffer plus 20 mM imidazole. The recombinant protein was then eluted using lysis buffer plus 200 mM imidazole. The elution fractions were then incubated with 5% (w/w) tobacco etch virus protease in order to cleave the N-terminal MBP expression tag and the mixture was dialyzed against a buffer containing 20 mM HEPES pH 8.0, 200 mM NaCl, and 2 mM DTT. MBP was then removed from the solution using another round of Ni-NTA purification. Proteins were then checked for purity using sodium dodecyl sulfate-polyacrylamide gel electrophoresis and pure fractions were concentrated in an Amicon Ultracel concentrator (Millipore), flash frozen in liquid nitrogen, and stored at −80 ˚C. For crystallography, fractions containing TrioCΔC were thawed from −80 ˚C on ice, and polished using gel filtration chromatography on a Superdex 75 10/300GL column (General

Electric healthcare) in a buffer containing 20 mM HEPES pH 8.0, 100 mM NaCl, and 2 mM DTT. Fractions containing TrioCΔC were then concentrated using an Amicon Ultracel concentrator before setting trays. Human RhoA was purified in a similar manner to that described above with the addition of 3 mM $MgCl_2$ and 10 μM GDP in all buffer solutions. (13) $G\alpha_qΔN$ was purified as described previously (30). Protein concentrations were evaluated using 280 nm absorbance (A_{280}) on an ND-1000 (NanoDrop Technologies) and standardized using extinction coefficients generated by the ProtParam ExPASy webserver (30).

TrioC crystallization

TrioCΔC crystals were grown at 20 ˚C using hanging drop vapor diffusion in 24-well VDX plates (Hampton Research). The drop contained 2 μL of 2 mg/mL protein mixed with 2 μL of well solution containing 100 mM HEPES pH 7.5 and 14% polyethylene glycol 3350 and 1 μL of double distilled H_2O. Crystals grew over a course of 2 d and took the form of 3 dimensional plates of about 25×100×300 μm. Crystals were transferred directly from the drop-in nylon cryoloops and plunged into liquid N_2 for data collection.

Data collection and processing

Diffraction data were collected at 110 K on the Life Sciences Collaborative Access Team beamline 21-ID-G at the Advanced Photon Source at Argonne National Laboratory and reduced, indexed, integrated, and scaled using the HKL2000 software package[13]. Statistics are shown in Table 1. Initial phases were provided using molecular replacement in Phaser[14] with Chainsaw[15] processed versions of the individual DH and PH domains of p63RhoGEF (PDB 2RGN) as sequential search models. Initial rounds of refinement consisted of model building in Coot[16] alternating with reciprocal space refinement in the PHENIX software package[17] using simulated annealing and torsional non-crystallographic symmetry (NCS) to restrain the three copies of TrioC in the asymmetric unit. Final rounds of refinement consisted of manual model building in Coot, and refinement using REFMAC5 (31) with manual X-ray weighting and translation-libration-screw refinement. NCS restraints were omitted in the final rounds to allow for minor variations between chains. Structure validation was performed using built in validation tools in Coot, the MolProbity server (32), and the PDB_REDO webserver (33). Refinement statistics are shown in Table 1. The TrioCΔC coordinates have been deposited into the PDB under accession code 6D8Z.

Structural comparisons

Unless stated otherwise, Chain A of the TrioC structure was used for comparisons. Chain B of PDB entry 2RGN was used for models of p63RhoGEF. Chain A of PDB entry 1RJ2 was used as a model for Dbs, and Chain A of PDB entry 1LB1 was used for RhoA-bound Dbs. Comparisons were made using the PyMOL Molecular Graphics System, Version 1.8.6.2, Schrodinger, LLC. The script Rotation Axis.py was used to calculate angles of rotation.

Differential scanning fluorimetry (DSF)

DSF experiments were performed first on a ThermoFluor plate reader (Johnson & Johnson) using 8-anilinonaphthalene-1-sulfonic acid as the fluorescent dye (WT TrioC T_m= 44.8 °C

with a 95% CI of [44.4, 45.3], N=11 independent experiments in at least duplicate). Data were also collected on 7900HT Fast Real-Time PCR system (Applied Biosystems) or a QuantStudio 6 Real-Time PCR system (Applied BioSystems) using Sypro Orange (SO) dye (ThermoFisher) (WT TrioC T_m= 49.4 °C with a 95% CI of [49.2, 49.7], N=15 independent experiments in at least duplicate). Although the absolute T_m for WT TrioC was different for each dye, we tested TrioC WT and R2150E and found ΔT_m for R2150E (T_m R2150E - T_m WT) was similar: +0.9 °C on the ThermoFluor instrument, and +0.6 °C on the PCR instruments (N=3 independent experiments performed in at least duplicate). Purified TrioC variants were incubated at 0.2 mg/mL in a buffer containing 20 mM HEPES pH 8.0, 200mM NaCl, and 2mM DTT with dye. Black 384 well PCR plates (Applied Biosystems) were used for the ThermoFlour instrument and wells were covered with silicon oil. For the QPCR instruments, white 384 well PCR plates (Applied Biosystems) were used and covered with sealing tape. These plates were exposed to a temperature gradient of 20–60 °C. Fluorescence was monitored as a function of temperature, and the T_m was determined by fitting the fluorescence data to a sigmoidal curve and calculating the inflection point in GraphPad Prism.(12,34, 35, 36)

Förster resonance energy transfer (FRET) nucleotide exchange assay

FRET was used to assess the nucleotide exchange activity of TrioC variants.(13, 37) First, 3 μM RhoA·GDP was incubated with 500 nM TrioC variants for 5 min at room temperature. Immediately before measurement, 1 μM 2′/3′-O-(N-Methyl-anthraniloyl)-guanosine-5′-triphosphate (MANT-GTP) (Jena Biosciences), was injected to a final assay volume of 100 μL. The mixture was then excited at 280 nm, and fluorescence intensity at 450 nm was read in 2 s intervals on a Flexstation 3 plate reader until a plateau was reached (~30 min). Fluorescence curves were then fit to a one-phase exponential association model using GraphPad Prism. The resulting k_{obs} were then compared to that of matched TrioC WT rates with a representative rate constant of (0.004 ± 0.0006 s^{-1}, N=3 independent experiments in triplicate). The 2152**Δ** and 2147**Δ** variants displayed an exchange rate too fast to be measured under the initial assay conditions. Thus, the exchange rate of these variants was measured using 50 nM GEF, and all relative rates are therefore reported as specific activities. Prior literature suggests that under our assay conditions the nucleotide exchange reaction rate is linear with respect to GEF concentration (6). For $G\alpha_q$ activation assays displayed in table 2, TrioC WT and variants were added at 250 nM GEF concentration (in order to lower the observed basal rate and better capture activation), $G\alpha_q$ at 550nM, and the assay was run with and without the addition of 30 μM $AlCl_3$ and 10mM NaF to generate AlF_4^- in solution.

Hydrogen-deuterium exchange mass spectrometry

First, 1 μL of 2.6 mg/ml TrioC in 20 mM HEPES pH 7.5, 50 mM NaCl, and 2 mM DTT was mixed with 15 μL of a buffer containing 8.3mM tris(hydroxymethyl)aminomethane (Tris) and 50mM NaCl at pH 7.2 at 0 °C, and 24 μL of ice cold quench buffers containing 0.1 M glycine pH 2.4, 16.6% (v/v) glycerol and various concentrations of guanidinium HCl (0.08, 0.8, 1.6 and 3.2 M) were then added. The quenched samples were then subjected to an immobilized pepsin column (16 μL bed volume) on ice at a flow rate of 20 μL/min for inline digestion. Proteolytic products were collected on a trap column for desalting and liquid chromatography-mass spectrometry (LC-MS) analysis was performed using an Agilent

Poroshell C18 column (EC-C18, 35×0.3mm, 2.7 μm) with a linear acetonitrile gradient (6.4%-38.4% over 30 min). Both trap and C18 columns were kept at 0 °C. MS analysis was done using an OrbiTrap Elite Mass Spectrometer (Thermo Fisher Scientific), and MS/MS data were searched against TrioC sequence by Proteome Discoverer (Thermo Fisher Scientific). Coverage maps of identified peptides were compared with each other and the 1.6 M GuHCl quench buffer was selected for further HDX-MS experiments. This enabled us to determine the proper quench buffer concentration for the HDX experiments.

All exchange stock solutions were kept on ice and contained 1.0 mg/mL of each TrioC variant, 8.3 mM Tris pH 7.2 and 50 mM NaCl. HDX-MS experiments were initiated by adding 48 μL of exchange stock solutions to 144 μL of D_2O buffer (8.3mM Tris, 50mM NaCl, pD 7.2) and quenching the reaction at varied time points (10, 100, 1000, 10,000 and 100,000 s) at 0 °C. At the indicated time, 16 μL of exchange reaction solution was taken out and mixed with 24 μL of ice cold quench buffer (0.1 M glycine pH 2.4, 16.6% (v/v) glycerol, 1.6 M GuHCl) and immediately frozen on dry ice. Non-deuterated and equilibrium deuterated control samples were also prepared for back exchange correction. All frozen samples were thawed at 4 °C and subjected to the above system for enzymatic digestion, LC separation and MS analysis. All the columns were kept at 0 °C to minimize back exchange. The extent of deuterium incorporation of deuterated peptides was determined using HDXaminer (Sierra Analytics, LLC, Modesto, CA), which calculates centroid deuterium incorporation values for each peptide. Ribbon maps were generated with in-house Excel macro and MatLab scripts.

Rhotekin pulldown assay

HEK293 cells cultured in Dulbecco's modified eagle medium plus 10% Fetal bovine serum (Sigma) in 15 cm dishes were cultured to 70% confluency and transfected with 15 μg deoxyribonucleic acid (DNA) encoding TrioFL wild type and variants using Turbofect transfection reagent (Thermo Fisher) at a 1:2 ratio of DNA to Turbofect. Active Rho levels were measured using the RhoA Pull-Down Activation Assay Biochem Kit (bead pull-down format) following manufacturer's instructions (Cytoskeleton, Inc.). Briefly, 24 h after transfection, cells were serum starved for an additional 24 h and lysed using provided lysis buffer. Protein concentrations were quantified using DC Protein Assay (BioRad), samples were adjusted to the same concentration using provided lysis buffer and then snap frozen in liquid N_2. Lysate with 600 μg of protein was added to 30 μL GST-tagged Rhotekin-RBD protein bound to sepharose beads. Samples were incubated while rocking at 4 °C for 1.5 h. Beads were then washed, eluted in Laemmli sample buffer, and analyzed by western blot using a mouse monoclonal anti-RhoA antibody (Cytoskeleton, Inc. Cat # ARH04) to measure the ratio of active to total RhoA. Bands were quantified using ImageJ software (NIH).

Statistical analysis

DSF and FRET nucleotide exchange experiments described above were performed in 3 experiments in at least duplicate. For DSF assays, average T_m values from each experiment for each variant were subtracted from compiled WT values obtained on the same instrument to obtain ΔT_m. Statistical significance was assessed using a one-way ANOVA test with a

post-hoc Dunnett's test for multiple comparisons to compare N=3 experiments of each variant with N=11 WT experiments (J&J Thermofluor) or N=15 experiments (qPCR instruments). For FRET activity assays comparing TrioC variants to WT, k_{obs} values for each variant were normalized to matched WT k_{obs} for each experimental N to generate fold GEF activation values for each variant. To capture the statistical spread in WT measurements, each experimental WT k_{obs} was normalized to the average WT k_{obs} of the N=3 experiments. Statistical significance was assessed using a one-way ANOVA test with a post-hoc Dunnett's test for multiple comparisons to compare N=3 fold GEF activation values of each variant with N=51 WT fold GEF activation values. For $G\alpha_q{\cdot}GDP{\cdot}AlF_4^-$ activation assays, k_{obs} in the presence of $G\alpha_q{\cdot}GDP{\cdot}AlF_4^-$ for each variant was normalized to k_{obs} in the presence of $G\alpha_q{\cdot}GDP$ to generate fold activation values. The fold $G\alpha_q{\cdot}GDP{\cdot}AlF_4^-$ activation value for TrioC WT was compared to cancer variants using a one-way ANOVA test with a post-hoc Dunnett's test for multiple comparisons. Errors are provided as 95% confidence intervals. Rhotekin assay data for Trio variants profiled in N=3 were normalized to the average of N=3 Trio WT values and then compared to the average Trio WT value using a one-way ANOVA test with a post-hoc Dunnett's test. Analysis was performed using GraphPad Prism version 7.00.

Supplementary Material

Refer to Web version on PubMed Central for supplementary material.

Acknowledgments:

The authors thank the Ginsburg and Lin laboratories for use of their QPCR instruments, and the University of Michigan Center for Structural Biology and High-Throughput Protein Production Facility for use of their Thermofluor instrument.

Funding: This work was supported by National Institutes of Health (NIH; grant CA221289 to J.S.G and J.J.G.T, grants HL122416 and HL071818 to J.J.G.T.; grants 5T32GM007767-38, 5T32GM007767-39, and F31CA224804 to S.J.B.; and grant 5T32GM007752-39 to N.A.). This research used resources of the Advanced Photon Source, a U.S. Department of Energy (DOE) Office of Science User Facility operated for the DOE Office of Science by Argonne National Laboratory under Contract No. DE-AC02-06CH11357. Use of the LS-CAT Sector 21 was supported by the Michigan Economic Development Corporation and the Michigan Technology Tri-Corridor (grant 085P1000817).

REFERENCES AND NOTES

1. Aittaleb M, Boguth CA, Tesmer JJG, Structure and Function of Heterotrimeric G Protein-Regulated Rho Guanine Nucleotide Exchange Factors, Molecular Pharmacology 77, 111–125 (2010). [PubMed: 19880753]
2. Cherfils J, Zeghouf M, Regulation of Small GTPases by GEFs, GAPs, and GDIs, Physiological Reviews 93, 269–309 (2013). [PubMed: 23303910]
3. Schmidt S, Debant A, Function and regulation of the Rho guanine nucleotide exchange factor Trio, Small GTPases 5, e983880 (2014).
4. Williams SL, Lutz S, Charlie NK, Vettel C, Ailion M, Coco C, Tesmer JJG, Jorgensen EM, Wieland T, Miller KG, Trio's Rho-specific GEF domain is the missing G q effector in C. elegans, Genes & Development 21, 2731–2746 (2007). [PubMed: 17942708]
5. Rojas RJ, Yohe ME, Gershburg S, Kawano T, Kozasa T, Sondek J, G q Directly Activates p63RhoGEF and Trio via a Conserved Extension of the Dbl Homology-associated Pleckstrin Homology Domain, J. Biol. Chem. 282, 29201–29210 (2007). [PubMed: 17606614]

6. Lutz S, Shankaranarayanan A, Coco C, Ridilla M, Nance MR, Vettel C, Baltus D, Evelyn CR, Neubig RR, Wieland T, Tesmer JJG, Structure of Galphaq-p63RhoGEF-RhoA complex reveals a pathway for the activation of RhoA by GPCRs, Science 318, 1923–1927 (2007). [PubMed: 18096806]
7. Vaque JP, Dorsam RT, Feng X, Iglesias-Bartolome R, Forsthoefel DJ, Chen Q, Debant A, Seeger MA, Ksander BR, Teramoto H, Gutkind JS, A Genome-wide RNAi Screen Reveals a Trio-Regulated Rho GTPase Circuitry Transducing Mitogenic Signals Initiated by G Protein-Coupled Receptors, Molecular Cell 49, 94–108 (2013). [PubMed: 23177739]
8. Van Raamsdonk CD, Bezrookove V, Green G, Bauer J, Gaugler L, O'Brien JM, Simpson EM, Barsh GS, Bastian BC, Frequent somatic mutations of GNAQ in uveal melanoma and blue naevi, Nature 457, 599–603 (2009). [PubMed: 19078957]
9. Van Raamsdonk CD, Griewank KG, Crosby MB, Garrido MC, Vemula S, Wiesner T, Obenauf AC, Wackernagel W, Green G, Bouvier N, Sozen MM, Baimukanova G, Roy R, Heguy A, Dolgalev I, Khanin R, Busam K, Speicher MR, O'Brien J, Bastian BC, Mutations in GNA11 in uveal melanoma, N. Engl. J. Med. 363, 2191–2199 (2010). [PubMed: 21083380]
10. Rossman KL, Der CJ, Sondek J, GEF means go: turning on RHO GTPases with guanine nucleotide-exchange factors, Nat Rev Mol Cell Biol 6, 167–180 (2005). [PubMed: 15688002]
11. Rossman KL, Worthylake DK, Snyder JT, Siderovski DP, Campbell SL, Sondek J, A crystallographic view of interactions between Dbs and Cdc42: PH domain-assisted guanine nucleotide exchange, The EMBO Journal 21, 1315–1326 (2002). [PubMed: 11889037]
12. Cash JN, Davis EM, Tesmer JJG, Structural and Biochemical Characterization of the Catalytic Core of the Metastatic Factor P-Rex1 and Its Regulation by PtdIns(3,4,5)P3, Structure/Folding and Design 24, 730–740 (2016). [PubMed: 27150042]
13. Kristelly R, Gao G, Tesmer JJG, Structural Determinants of RhoA Binding and Nucleotide Exchange in Leukemia-associated Rho Guanine-Nucleotide Exchange Factor, J. Biol. Chem. 279, 47352–47362 (2004). [PubMed: 15331592]
14. Chhatriwala MK, Betts L, Worthylake DK, Sondek J, The DH and PH Domains of Trio Coordinately Engage Rho GTPases for their Efficient Activation, Journal of Molecular Biology 368, 1307–1320 (2007). [PubMed: 17391702]
15. Nimnual AS, Yatsula BA, Bar-Sagi D, Coupling of Ras and Rac guanosine triphosphatases through the Ras exchanger Sos, Science 279, 560–563 (1998). [PubMed: 9438849]
16. Zheng J, Chen RH, Corblan-Garcia S, Cahill SM, Bar-Sagi D, Cowburn D, The solution structure of the pleckstrin homology domain of human SOS1. A possible structural role for the sequential association of diffuse B cell lymphoma and pleckstrin homology domains, J. Biol. Chem. 272, 30340–30344 (1997). [PubMed: 9374522]
17. Shankaranarayanan A, Boguth CA, Lutz S, Vettel C, Uhlemann F, Aittaleb M, Wieland T, Tesmer JJG, Gαq allosterically activates and relieves autoinhibition of p63RhoGEF, Cellular Signalling 22, 1114–1123 (2010). [PubMed: 20214977]
18. Carvajal RD, Piperno-Neumann S, Kapiteijn E, Chapman PB, Frank S, Joshua AM, Piulats JM, Wolter P, Cocquyt V, Chmielowski B, Evans TRJ, Gastaud L, Linette G, Berking C, Schachter J, Rodrigues MJ, Shoushtari AN, Clemett D, Ghiorghiu D, Mariani G, Spratt S, Lovick S, Barker P, Kilgour E, Lai Z, Schwartz GK, Nathan P, Selumetinib in Combination With Dacarbazine in Patients With Metastatic Uveal Melanoma: A Phase III, Multicenter, Randomized Trial (SUMIT), JCO 36, 1232–1239 (2018).
19. Yu OM, Brown JH, G Protein-Coupled Receptor and RhoA-Stimulated Transcriptional Responses: Links to Inflammation, Differentiation, and Cell Proliferation, Molecular Pharmacology 88, 171–180 (2015). [PubMed: 25904553]
20. Sahai E, Marshall CJ, RHO–GTPASES AND CANCER, Nat Rev Cancer 2, 133–142 (2002). [PubMed: 12635176]
21. Vega FM, Ridley AJ, Rho GTPases in cancer cell biology, FEBS Lett. 582, 2093–2101 (2008). [PubMed: 18460342]
22. Worthylake DK, Rossman KL, Sondek J, Crystal Structure of the DH/PH Fragment of Dbs without Bound GTPase, Structure 12, 1079–1086 (2004).

23. Cerami E, Gao J, Dogrusoz U, Gross BE, Sumer SO, Aksoy BA, Jacobsen A, Byrne CJ, Heuer ML, Larsson E, Antipin Y, Reva B, Goldberg AP, Sander C, Schultz N, The cBio Cancer Genomics Portal: An Open Platform for Exploring Multidimensional Cancer Genomics Data: Figure 1, Cancer Discovery 2, 401–404 (2012). [PubMed: 22588877]
24. Feng X, Degese MS, Iglesias-Bartolome R, Vaque JP, Molinolo AA, Rodrigues M, Zaidi MR, Ksander BR, Merlino G, Sodhi A, Chen Q, Gutkind JS, Hippo-Independent Activation of YAP by the GNAQ Uveal Melanoma Oncogene through a Trio-Regulated Rho GTPase Signaling Circuitry, CCELL 25, 831–845 (2014).
25. Soisson SM, Nimnual AS, Uy M, Bar-Sagi D, Kuriyan J, Crystal structure of the Dbl and pleckstrin homology domains from the human Son of sevenless protein, Cell 95, 259–268 (1998). [PubMed: 9790532]
26. Yoshizuka N, Moriuchi R, Mori T, Yamada K, Hasegawa S, Maeda T, Shimada T, Yamada Y, Kamihira S, Tomonaga M, Katamine S, An Alternative Transcript Derived from the TrioLocus Encodes a Guanosine Nucleotide Exchange Factor with Mouse Cell-transforming Potential, J. Biol. Chem. 279, 43998–44004 (2004). [PubMed: 15308664]
27. van Unen J, Botman D, Yin T, Wu YI, Hink MA, Gadella TWJ, Postma M, Goedhart J, The C-terminus of the oncoprotein TGAT is necessary for plasma membrane association and efficient RhoA-mediated signaling, BMC Cell Biol 19, 1–15 (2018). [PubMed: 29433423]
28. Yamada K, Moriuchi R, Mori T, Okazaki E, Kohno T, Nagayasu T, Matsuyama T, Katamine S, Tgat, a Rho-specific guanine nucleotide exchange factor, activates NF-κB via physical association with IκB kinase complexes, Biochemical and Biophysical Research Communications 355, 269–274 (2007). [PubMed: 17292329]
29. Mori T, Moriuchi R, Okazaki E, Yamada K, Katamine S, Tgat oncoprotein functions as a inhibitor of RECK by association of the unique C-terminal region, Biochemical and Biophysical Research Communications 355, 937–943 (2007). [PubMed: 17328864]
30. Wilkins MR, Gasteiger E, Bairoch A, Sanchez JC, Williams KL, Appel RD, Hochstrasser DF, Protein identification and analysis tools in the ExPASy server, Methods Mol. Biol. 112, 531–552 (1999). [PubMed: 10027275]
31. Murshudov GN, Vagin AA, Dodson EJ, Refinement of Macromolecular Structures by the Maximum-Likelihood Method, Acta Cryst (1997). D53, 240–255, 1–16 (1997).
32. Chen VB, Arendall WB, Headd JJ, Keedy DA, Immormino RM, Kapral GJ, Murray LW, Richardson JS, Richardson DC, MolProbity: all-atom structure validation for macromolecular crystallography, Acta Cryst (2010). D66, 12–21, 1–10 (2009).
33. Joosten RP, Long F, Murshudov GN, Perrakis A, The PDB_REDO server for macromolecular structure model optimization, IUCrJ (2014). M1, 213–220, 1–8 (2014).
34. Mezzasalma TM, Kranz JK, Chan W, Struble GT, Schalk-Hihi C, Deckman IC, Springer BA, Todd MJ, Enhancing Recombinant Protein Quality and Yield by Protein Stability Profiling, Journal of Biomolecular Screening 12, 418–428 (2007). [PubMed: 17438070]
35. Homan KT, Waldschmidt HV, Glukhova A, Cannavo A, Song J, Cheung JY, Koch WJ, Larsen SD, Tesmer JJG, Crystal Structure of G Protein-coupled Receptor Kinase 5 in Complex with a Rationally Designed Inhibitor, J. Biol. Chem. 290, 20649–20659 (2015). [PubMed: 26032411]
36. Lyon AM, Begley JA, Manett TD, Tesmer JJG, Molecular Mechanisms of Phospholipase C β 3 Autoinhibition, Structure/Folding and Design 22, 1844–1854 (2014). [PubMed: 25435326]
37. Brecht M, Sewald K, Schiene K, Keen G, Fricke M, Sauer M, Niehaus K, The use of surface plasmon resonance (SPR) and fluorescence resonance energy transfer (FRET) to monitor the interaction of the plant G-proteins Ms-Rac1 and Ms-Rac4 with GTP, Journal of Biotechnology 112, 151–164 (2004). [PubMed: 15288950]

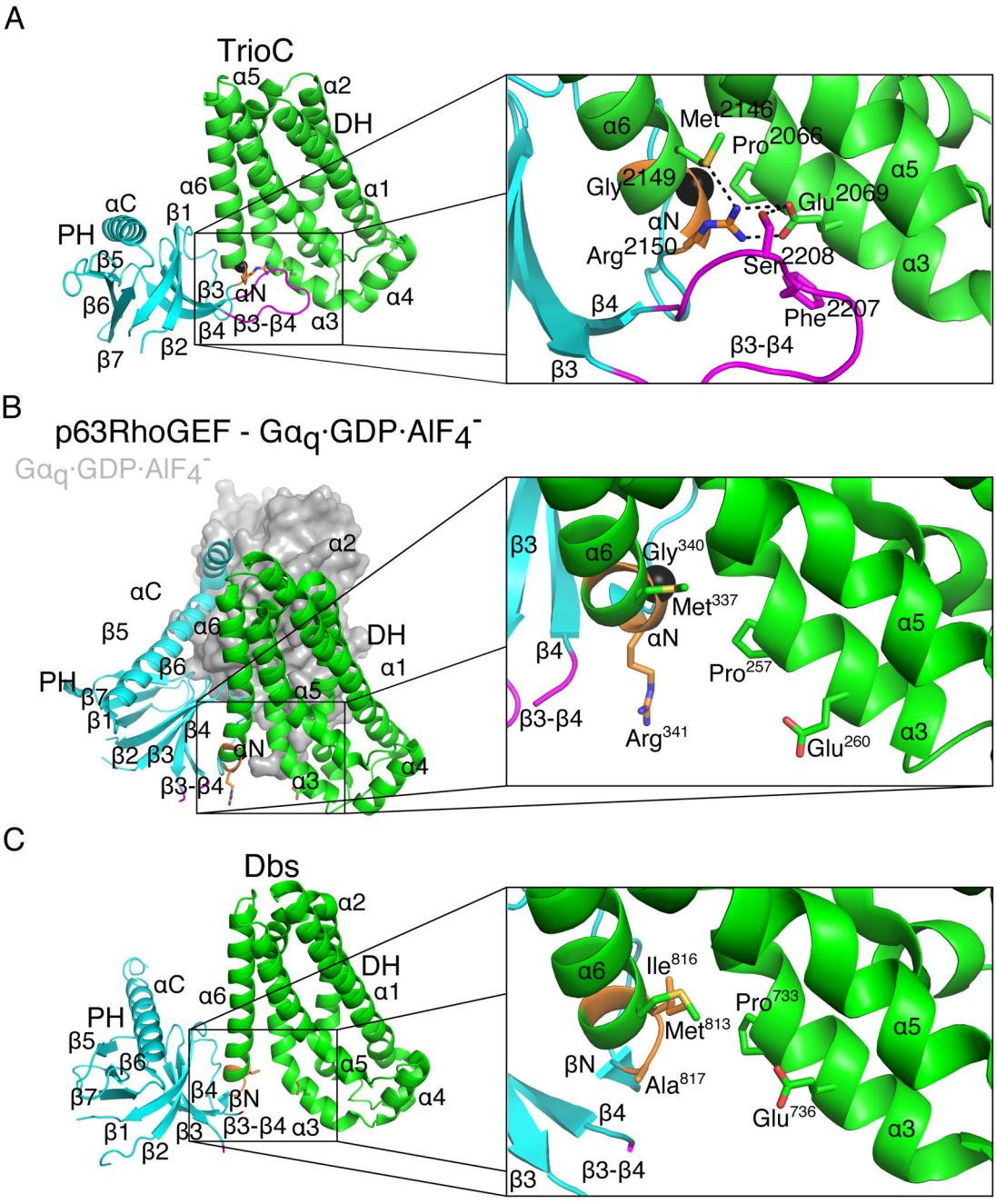

Figure 1. Structural overview of the DH-PH interface found in TrioC in comparison with related DH/PH modules.

(**A**) Overall domain orientation and structural layout of the autoinhibited TrioC DH/PH module. The DH domain is shown in green and is composed of α-helical segments α1-α6. The PH domain is shown in cyan and is composed of αN and αC helices and β-strands 1-7. αN is colored orange, and the β3-β4 loop magenta. (**B and C**) For comparison, the structures for active p63RhoGEF (PDB entry 2RGN) (B) and Dbs (PDB entry 1RJ2) (C) were aligned to TrioC based on their DH domains. Insets highlight the side chains of key residues in the DH-PH interface as sticks, except for Gly^{2149} in TrioC and Gly^{340} in

p63RhoGEF, whose Cα atoms are shown as black spheres. In (B), $G\alpha_q$·GDP·AlF_4^- is shown as a grey surface representation, and RhoA is omitted for clarity. In (B) and (C), the β3-β4 loops are partially disordered.

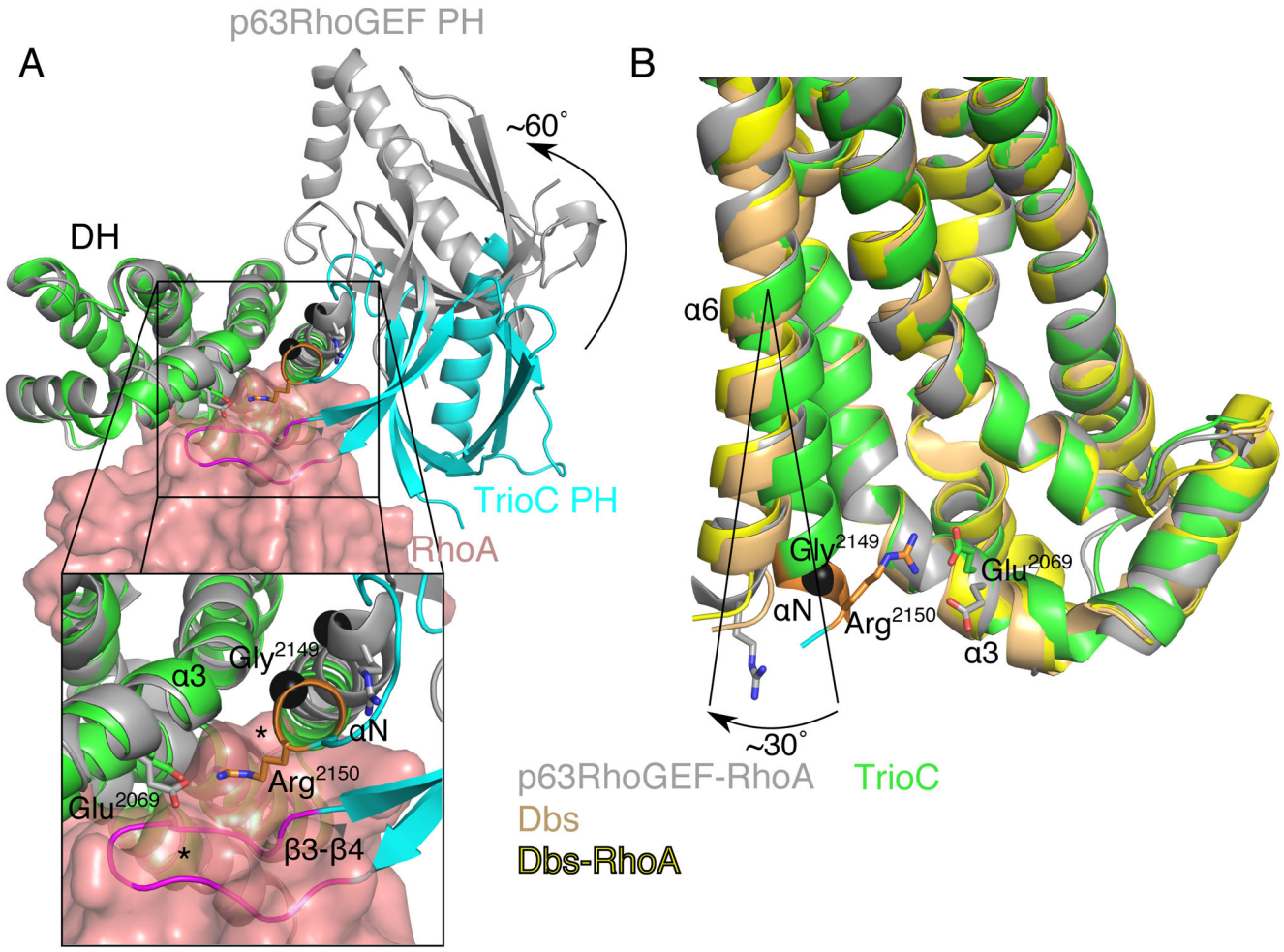

Figure 2. Conformational changes that lead to occlusion of the RhoA binding site in TrioC.

(A) TrioC is shown aligned with the activated structure of p63RhoGEF using their DH domains. TrioC exhibits a 60° rotation of its PH domain (cyan) relative to that of activated p63RhoGEF (dark grey). Inset, the observed conformation of TrioC forms steric overlaps with the RhoA binding site in two key regions, α6-αN, and β3-β4, demarcated by asterisks. **(B)** The α6-αN junction also bends towards the DH domain by 30˚ in autoinhibited TrioC relative to related DH/PH structures of known structure. Overlaid are the hinge regions of autoinhibited TrioC, $G\alpha_q$-p63RhoGEF-RhoA (PDB entry 2RGN), Dbs (PDB entry 1RJ2), and Dbs–RhoA (PDB entry 1LB1). Key TrioC residues are shown as sticks or spheres, as in Figure 1. The analogous residues in p63RhoGEF are also shown.

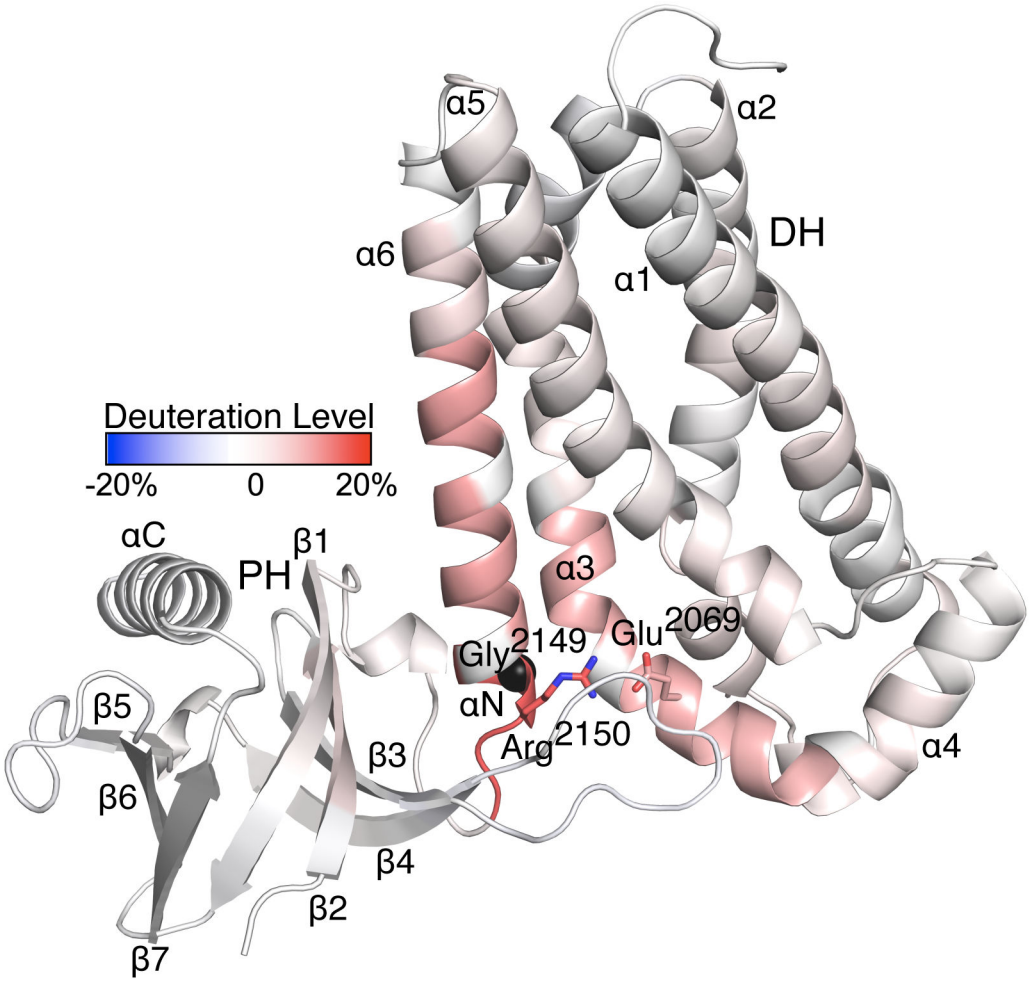

Figure 3. HDX-MS solution dynamics of the activated R2150W variant suggests physical separation of the DH and PH domains.

Difference in HDX rates (TrioC R2150W-Trio WT) were used to color the Cα atoms in the TrioC crystal structure. Scale bar indicates the color that corresponds to a given rate of exchange, with red indicating more exchange in the variant compared to the WT. The side chains of Glu^{2069} and Arg^{2150} are shown as sticks, and the Cα atom of Gly^{2149} as a sphere. Data are the mean of N=2 experiments (using protein from independent purifications) using matched peptides from HDXaminer and averaged over five time points. Plots of HDX on the primary structures of TrioC WT and R2150W are shown in figure S3.

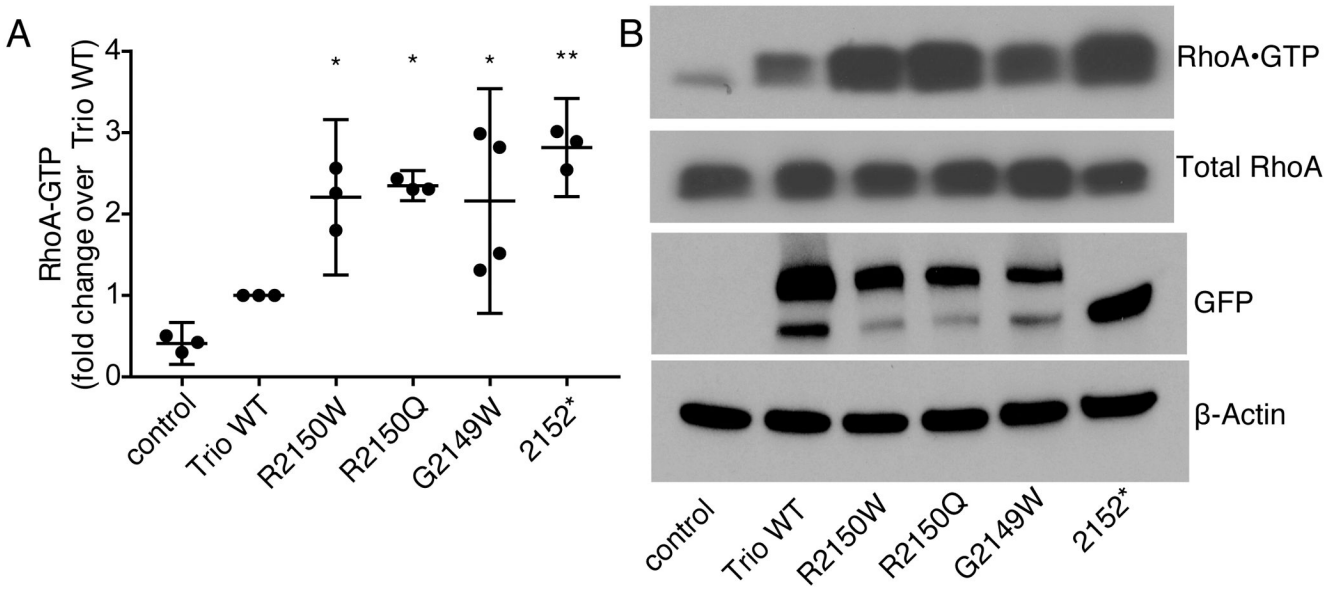

Figure 4. Trio mutants found in patient tumors activate RhoA in HEK293 cells.

(A) Quantification of N = 3 (N=4 for G2149W) independent biological Rhotekin pulldown experiments for control condition (pEGFP-C1), Trio WT, and Trio variants with error shown as 95% confidence intervals. Blots for RhoA·GTP were normalized using total RhoA content in cell lysate. Statistical comparisons to Trio WT were made using a one-way ANOVA test with a post-hoc Dunnett's test for multiple comparisons. * refers to $p<0.05$ and ** to $p<0.01$. **(B)** Representative Western blot images from one of the three experiments. The top two blots show RhoA·GTP and total RhoA content, respectively. The third blot shows Trio variant expression, blotting for the eGFP fusion partner, with β-actin used as a loading control. Quantitative comparison of Trio variant expression over 3 independent biological experiments is shown in figure S5. A minor truncation product of full-length Trio was present.

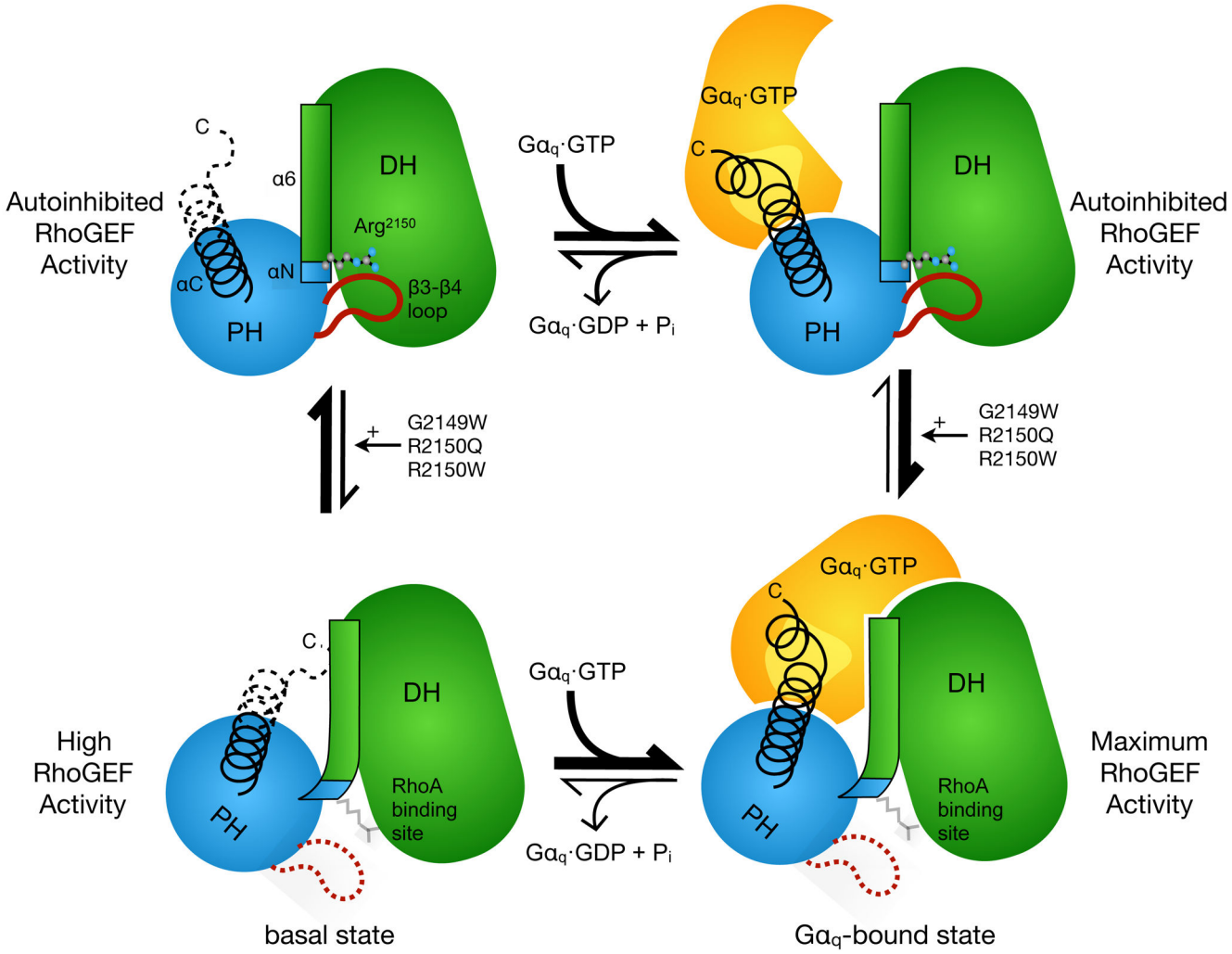

Figure 5. Model for TrioC activation.

TrioC exists in a conformational equilibrium between inactive and active states that can be biased towards the active state by either active $G\alpha_q$ or mutations in the DH-PH interface. The thicker half-arrows represent the favored direction in the equilibria. The DH domain is represented by a green oval with its RhoA binding site highlighted in yellow. α6 is shown as a green rectangle that forms a continuous helix with αN, represented as a blue rectangle. The PH domain is represented as a blue circle, with its C-terminal αC helix as a black helix. Arg^{2150} is shown as a ball-and-stick model, and the β3-β4 loop as a cartoon loop. $G\alpha_q$ is shown as a gold shape with its effector binding region in light yellow. Disorder is indicated with dashed lines and a blurring of Arg^{2150}. The autoinhibited conformation in the top left quadrant is represented by PDB 6D8Z and the maximum activity state is represented by PDB 2RGN, where $G\alpha_q$ binds to both the PH and DH domains and constrains them in a more open configuration that features a bent α6-αN helix.

Table 1.
Crystallographic data collection and refinement statistics.

X-ray crystallography data for TrioC. Parentheses indicate values for highest resolution shell. ND, not determined.

	TrioCΔC (human Trio 1960-2275)
Data collection statistics	
Synchrotron source	LS-CAT beamline 21-ID-G, Advanced Photon Source
Wavelength (Å)	0.97856
Resolution range (Å)	50-2.65 (2.70-2.65)
Space group	$P2_12_12_1$
Unit cell (a, b, c) (Å)	59.2, 85.8, 182.4
Unique reflections	30511 (1371)
Multiplicity	5.0 (3.8)
Completeness (%)	98.7 (90.1)
Mean I/σI	18.9 (1.2)
$CC_{1/2}$	ND (0.699)
R_{sym}	0.085 (0.746)
Refinement statistics	
Resolution limits (Å)	15-2.65 (2.70-2.65)
Number of test reflections	28787 (1862)
R_{work}	0.23 (0.34)
R_{free}	0.27 (0.37)
Number of nonhydrogen atoms	7525
Macromolecule	7499
Ligand	0
Water	26
Protein Residues	907
RMS bonds (Å)	0.008
RMS angles (°)	1.2
Ramachandran favored (%)	97.8
Ramachandran outliers (%)	0
Clashscore calculated from MolProbity	1.33
Average B-factor	76.0
Macromolecule	76.0
Ligand	N/A
Water	48.0

Table 2.
Biochemical analysis of the TrioC module.

DSF and GEF activation data for TrioC variants. ΔT_m= T_m(variant)-T_m(WT). Fold GEF activation= average k_{obs}(variant)/k_{obs}(WT). Fold activation by $G\alpha_q$·GDP·AlF_4^-= average k_{obs}(variant+$G\alpha_q$·GDP·AlF_4^-)/ k_{obs}(variant+$G\alpha_q$·GDP). ND= not determined. Each variant was profiled in N=3 experiments, each performed at least in technical duplicate. A one-way ANOVA with post Dunnett's test was used to test for significance for ΔT_m, fold GEF activation, and $G\alpha_q$·GDP·AlF_4^- activation for each variant in comparison to WT;

Variant	ΔTm (°C)	95% CI for ΔTm	GEF activation (Fold/WT)	95% CI for GEF activation	Fold activation by $G\alpha_q$·GDP·AlF_4^-	95% CI for Fold activation by $G\alpha_q$·GDP·AlF_4^-
WT	0.0	[−0.5,0.5]#	1.0	[0.9, 1.1]	3.1	[0.4, 5.9]
E2069A	−6.0***	[−7.3, −4.7]	0.7	[0.1, 1.3]	ND	ND
M2146A	−3***	[−3.6, −2.4]	0.8	[−0.5, 2.2]	ND	ND
S2208A	−3.2***	[−4.8, −1.7]	1.4	[0.1, 2.7]	ND	ND
R2150A	0.9*	[−0.2, 1.9]	0.9	[0.03, 1.8]	ND	ND
F2207A	1.1	[−0.6, 2.8]	0.7	[−0.1, 1.6]	ND	ND
Δ2204-2208	−0.4	[−1.1, 0.2]	1.5	[0.2, 2.8]	ND	ND
Δ2203-2209	−0.5	[−0.9, −0.1]	1.0	[−0.5, 2.7]	ND	ND
G2149I	−6.3***	[−6.7, −5.9]	1.9	[−0.7, 4.6]	ND	ND
E2069R/R2150E	−7.9***	[−14, −2.2]	3.2**	[1.6, 4.7]	ND	ND
R2150E	0.9	[0.7, 1.1]	1.0	[−0.4, 2.4]	ND	ND
2153Δ	ND	ND	3.0*	[0.7, 5.3]	ND	ND
2152Δ	ND	ND	11***	[4.5, 18]	ND	ND
2147Δ	ND	ND	14***	[4.8, 22]	ND	ND
2143Δ	ND	ND	0.2	[−0.2, 0.6]	ND	ND
G2149W	−3.6***	[−3.9, −3.3]	4.3***	[2.4, 6.4]	1.5*	[0.7, 2.3]
R2150Q	−1.6***	[−3.3, 0.2]	4.5***	[2.1, 6.9]	2.2	[1.2, 3.1]
R2150W	−3.1***	[−5.1, −1.2]	9.3***	[−0.4, 18]	0.9**	[0.7, 1.0]

* P<0.05,

** P<0.01, and

*** P<0.005.

#, Data was collected using two experimental setups; the larger 95% CI was chosen here.

See the Methods section for further explanation of methods and statistical analysis used for this table.